Nucleation and growth in systems with two stable phases

R. M. Bradley
Department of Physics, Colorado State University, Fort Collins, Colorado 80523

P. N. Strenski
IBM Thomas J. Watson Research Center, P.O. Box 218, Yorktown Heights, New York 10598

(Received 19 May 1989)

We study nucleation and growth in systems with two distinct stable phases for both homogeneous and heterogeneous nucleation. Mean-field theories are developed that predict the fraction of material in each of the two stable phases as a function of time in any dimension d. Exact solutions for homogeneous and heterogeneous nucleation for $d=1$ are obtained and compared with the mean-field results. In the case of homogeneous nucleation in one dimension, we find an anomalous power-law correction to the leading-order asymptotic behavior for large times. The power-law exponent is a continuously varying function of the nucleation rates. Finally, Monte Carlo simulations show that the mean-field theories are surprisingly accurate for $d=2$.

I. INTRODUCTION

The Kolmogorov or Johnson-Mehl-Avrami model has been widely employed as a model of the kinetics of grain growth during the crystallization of amorphous solids.[1-10] It has also been applied to the kinetics of reconstructive first-order phase transitions[11,12] and to domain switching in ferroelectrics.[13,14] In the model, vanishingly small spherical grains nucleate at a constant rate per unit volume Γ in the metastable phase and grow isotropically at constant velocity v once formed. As first shown by Kolmogorov,[1] the volume fraction of untranformed material at time t is

$$\Phi(t)=\exp\left[-\frac{\Omega_d}{d+1}\Gamma v^d t^{d+1}\right], \tag{1.1}$$

where d is the dimension of space and Ω_d is the volume of a d-dimensional unit sphere. A very thorough discussion of the circumstances in which the Kolmogorov model can be applied may be found in Ref. 9.

The nucleation process in the Kolmogorov model is referred to as homogeneous because it occurs uniformly throughout the metastable phase. In many cases, however, the nucleation is heterogeneous: Nuclei form almost exclusively at impurities or defects which were present before the phase transformation began.[4] A simple but often-studied model of heterogeneous nucleation is obtained by randomly placing nuclei with density γ throughout the solid. When the phase transformation is initiated at $t=0$, spherical grains form at each nucleus and grow isotropically with velocity v. The volume fraction of untransformed material at time t is

$$\Phi(t)=\exp(-\Omega_d\gamma v^d t^d)\ . \tag{1.2}$$

There is a single stable phase in both these models. However, it is possible for a system to have two qualitatively different stable (or nearly stable) phases. In this paper we will study the kinetics of both homogeneous and heterogeneous nucleation in a system with two distinct stable phases A and B. In the case of homogeneous nucleation, the A and B phases will be taken to nucleate at rates Γ_A and Γ_B per unit volume of metastable phase. For heterogeneous nucleation, the densities of A and B nuclei will be denoted by γ_A and γ_B, respectively. An interface between the metastable and the A (B) phase will be taken to propagate with constant velocity v_A (v_B) once formed. An A-B interface, on the other hand, will fluctuate if both phases are stable and drift slowly if the free energy difference between the two phases is small. Here we will neglect interface fluctuations and the slow drift of A-B interfaces (if present) and treat these interfaces as stationary. In general, $\Gamma_A\neq\Gamma_B$, $\gamma_A\neq\gamma_B$, and $v_A\neq v_B$.[15] We may assume that $v_B\leq v_A$ without loss of generality.

Figure 1 shows the free energy density f as a function of the order parameter M for a model system in which there are two distinct stable phases A and B. If the system is initially in the metastable state $M=0$, grains of A and B phase will nucleate and grow. The nucleation rates

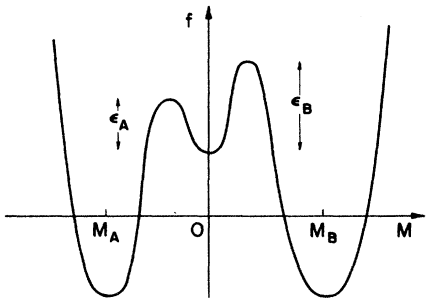

FIG. 1. Free energy density f as a function of the order parameter M for a model system with two distinct stable phases. $M=0$ is a metastable state, while $M=M_A$ and $M=M_B$ are stable. The barrier heights ϵ_A and ϵ_B may differ.

 ©1989 The American Physical Society

Γ_A and Γ_B for homogeneous nucleation differ if the barrier heights ϵ_A and ϵ_B are not the same. Similarly, in the case of heterogeneous nucleation, γ_A and γ_B need not be equal since different types of defects may nucleate one phase more readily than the other. Finally, the normal velocity of an interface between the metastable and A phases is[9]

$$v_A = L_A\{K + [f(0) - f(M_A)]/\sigma_A\} . \tag{1.3}$$

Here

$$K \equiv R_1^{-1} + \cdots + R_{d-1}^{-1} ,$$

where R_i is the ith principal curvature of the interface, σ_A is the surface free energy, and L_A is a kinetic coefficient. For grains much larger than a critical nucleus, the reduction of the interface velocity by the surface tension is negligible, and v_A is to a good approximation just the constant

$$L_A[f(0) - f(M_A)]/\sigma_A .$$

In the same way,

$$v_B \cong L_B[f(0) - f(M_B)]/\sigma_B$$

for sufficiently large B-phase grains. The kinetic coefficients L_A and L_B (and hence v_A and v_B) will be different if the A and B phases are not related by a symmetry operation. Our models of two-phase nucleation and growth are therefore expected to apply to systems of this kind, and in the most general case the parameters characterizing the A and B phases will differ.

A variety of other applications of the models can be envisioned. For example, the growth of a colony of sedentary organisms on a nutrient surface often starts from a "seed" or nucleus. A disk-shaped colony then spreads over the surface at constant velocity as the organisms reproduce. The colony expands isotropically until a point on its perimeter reaches a place which has already been occupied by a second colony. If the nutrient is randomly seeded at $t=0$, we have a realization of the model of heterogeneous one-phase nucleation described above. Homogeneous nucleation can be obtained by randomly scattering seeds over the surface at a constant rate while colonization proceeds, since a seed which lands on a previously occupied site does not produce a new colony. Two-phase nucleation and growth occurs if colonies of two different species of organisms compete for the same nutrient. Note that in general the growth rates of the two different kinds of colony will differ.

The paper is organized as follows. In Sec. II we develop a mean-field theory (MFT) for both homogeneous and heterogeneous two-phase nucleation and growth in d dimensions. The models are solved exactly in one dimension (1D) in Sec. III. For the homogeneous case in $d=1$, we find that the fraction of untransformed material $\Phi(t)$ has an anomalous power-law correction to the leading order long-time behavior

$$\Phi(t) \sim \exp[-(\Gamma_A + \Gamma_B)v_B t^2] .$$

In Sec. IV, Monte Carlo results in two dimensions (2D) are compared with the mean-field predictions. We give our conclusions in Sec. V.

II. MEAN-FIELD THEORIES

A. Heterogeneous nucleation

Before deriving the MFT for heterogeneous two-phase nucleation, it is helpful to first develop a MFT for heterogeneous one-phase nucleation. Accordingly, let $n(t) = 1 - \Phi(t)$ be the fraction of material which has been transformed at time t. If we ignore overlap of the growing spheres, then

$$n(t) = \gamma \Omega_d v^d t^d$$

and

$$\frac{dn}{dt} = \Omega_d d \gamma v^d t^{d-1} . \tag{2.1}$$

This is of course an overestimate of n: Material which has already been transformed cannot be transformed again. If we neglect spatial correlations, this may be taken into account by reducing dn/dt by a factor of $(1-n)$. Equation (2.1) then becomes

$$\frac{dn}{dt} = \Omega_d d \gamma v^d t^{d-1}(1-n) ,$$

or

$$\frac{d\Phi}{dt} = -\Omega_d d \gamma v^d t^{d-1} \Phi .$$

This has the solution

$$\Phi(t) = \exp(-\Omega_d \gamma v^d t^d) .$$

Comparing this with Eq. (1.2), we see that we have in fact obtained the exact result for heterogeneous one-phase nucleation.

This approach is readily generalized to heterogeneous two-phase nucleation. Arguing in the same way as above, we obtain the following mean-field equations for the fraction of material in the A phase, n_A, and in the B phase, n_B:

$$\frac{dn_A}{dt} = \Omega_d d \gamma_A v_A^d t^{d-1}(1 - n_A - n_B) \tag{2.2}$$

and

$$\frac{dn_B}{dt} = \Omega_d d \gamma_B v_B^d t^{d-1}(1 - n_A - n_B) . \tag{2.3}$$

To solve this system, let $\Phi = 1 - n_A - n_B$ be the untransformed fraction. Addition of Eqs. (2.2) and (2.3) then yields

$$\frac{d\Phi}{dt} = -\Omega_d d(\gamma_A v_A^d + \gamma_B v_B^d) t^{d-1} \Phi .$$

This has the solution

$$\Phi(t) = \exp[-\Omega_d(\gamma_A v_A^d + \gamma_B v_B^d) t^d] . \tag{2.4}$$

Inserting this in Eq. (2.2) and integrating, we have

$$n_A(t)=\frac{\gamma_A v_A^d}{\gamma_A v_A^d+\gamma_B v_B^d}\{1-\exp[-\Omega_d(\gamma_A v_A^d+\gamma_B v_B^d)t^d]\}\ . \tag{2.5}$$

In particular, the fraction in the A phase when the phase transformation is complete is given by

$$n_A(\infty)=\frac{\gamma_A v_A^d}{\gamma_A v_A^d+\gamma_B v_B^d}=\frac{1}{1+\bar{\gamma}\alpha^d}\ , \tag{2.6}$$

where $\bar{\gamma}\equiv\gamma_B/\gamma_A$ and $\alpha\equiv v_B/v_A$.

As will be discussed in detail below, the MFT for heterogeneous two-phase nucleation is not exact unless v_A and v_B happen to coincide. It does provide a good approximation in dimensions $d\geq 2$, however.

B. Homogeneous nucleation

The mean-field equations for homogeneous two-phase nucleation are obtained in a manner which is completely analogous to that employed in the preceding section. They are

$$\frac{dn_A}{dt}=\Omega_d\Gamma_A v_A^d t^d(1-n_A-n_B) \tag{2.7}$$

and

$$\frac{dn_B}{dt}=\Omega_d\Gamma_B v_B^d t^d(1-n_A-n_B)\ . \tag{2.8}$$

Adding these, we have

$$\frac{d\Phi}{dt}=-\Omega_d(\Gamma_A v_A^d+\Gamma_B v_B^d)t^d\Phi\ . \tag{2.9}$$

The solution to Eq. (2.9) is

$$\Phi(t)=\exp\left[-\frac{\Omega_d}{d+1}(\Gamma_A v_A^d+\Gamma_B v_B^d)t^{d+1}\right]\ . \tag{2.10}$$

The time dependence of n_A can now be obtained by inserting this into Eq. (2.7) and integrating. We find that

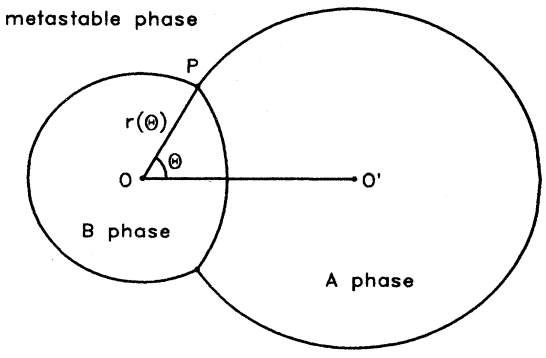

FIG. 2. Collision of an A-phase grain with nucleus at O' and a B-phase grain with nucleus at O. The A, B, and metastable phases touch at the point P, which has polar coordinates $(r(\theta),\theta)$.

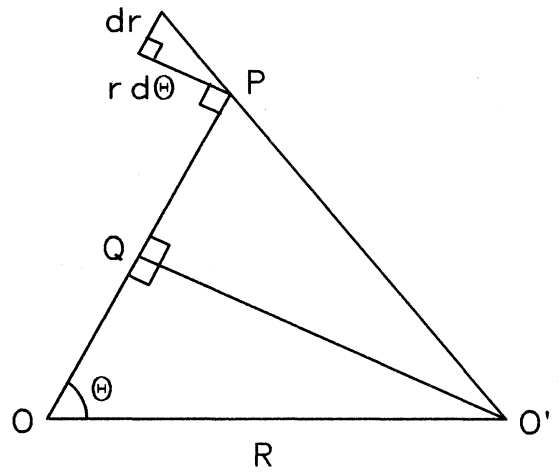

FIG. 3. Grain geometry when the line $O'P$ is tangent to the A-B interface at P. The nuclei of the A and B phase grains are at O' and O, respectively. The A, B, and metastable phases meet at P.

$$n_A(t)=\frac{\Gamma_A v_A^d}{\Gamma_A v_A^d+\Gamma_B v_B^d}\times\left[1-\exp\left[-\frac{\Omega_d}{d+1}(\Gamma_A v_A^d+\Gamma_B v_B^d)t^{d+1}\right]\right]\ . \tag{2.11}$$

The fraction of material in the A phase at $t=\infty$ is

$$n_A(\infty)=\frac{\Gamma_A v_A^d}{\Gamma_A v_A^d+\Gamma_B v_B^d}=\frac{1}{1+\bar{\Gamma}\alpha^d}\ , \tag{2.12}$$

where $\bar{\Gamma}\equiv\Gamma_B/\Gamma_A$.

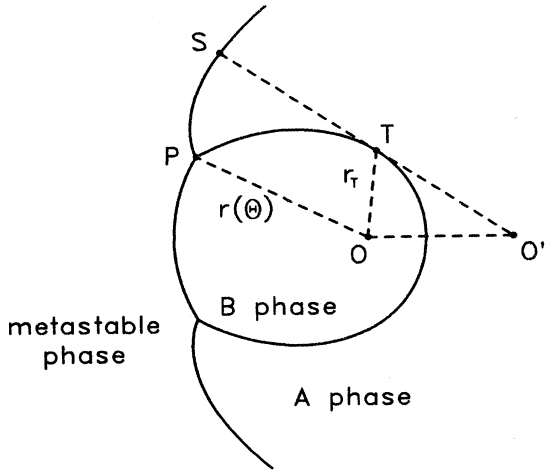

FIG. 4. Grain geometry for $\theta>\theta_T$. The points O, O', and P are as defined in Fig. 2. The line $O'S$ is tangent to the A-B interface at T.

C. Physical interpretation of the mean-field approximations

Our mean-field results are not exact unless $v_A = v_B$. To understand why this is so, consider the collision of two grains, one of A phase and the other of B phase. We will do this in two dimensions, since the problem is trivial in 1D, while the 2D result is easily generalized to higher dimensions. We will study the most general case in which the nucleation of the two grains need not occur at the same time.

Let the nucleus of the B-phase grain be at the point O. The nucleus of the A-phase grain will be taken to be a distance R away at O'. Finally, introduce polar coordinates with origin at O and the line between O and O' on the ray $\theta=0$. We shall find the equation of the interface between the two phases when the transformation is complete, $r = r(\theta)$.

Consider a time t after the grains first make contact at time $t = t_c$. Let P be the point in the upper half plane where the A, B, and metastable phases touch (see Fig. 2). Provided that the line $O'P$ lies entirely in the A phase and the line OP lies in the B phase, the distance $r(\theta)$ between O and P is given by

$$t - t_c = v_B^{-1}[r(\theta) - r(0)] = v_A^{-1}\{[R^2 + r^2(\theta) - 2Rr(\theta)\cos\theta]^{1/2} - [R - r(0)]\} . \tag{2.13}$$

Let $\rho(\theta) = r(\theta)/R$ and $\rho_0 = r(0)/R$. Rearranging Eq. (2.13), we obtain

$$[\alpha^{-1}(\rho - \rho_0) + 1 - \rho_0]^2 = 1 + \rho^2 - 2\rho\cos\theta \tag{2.14}$$

or

$$(1-\alpha^2)\rho^2(\theta) - 2(\rho_0 + \alpha\rho_0 - \alpha - \alpha^2\cos\theta)\rho(\theta) + (\rho_0 + \alpha\rho_0 - \alpha)^2 - \alpha^2 = 0 . \tag{2.15}$$

The root of this quadratic satisfying $\rho(0) = \rho_0$ is

$$\rho(\theta) = (1-\alpha^2)^{-1}(\rho_0 + \alpha\rho_0 - \alpha - \alpha^2\cos\theta) + (1-\alpha^2)^{-1}\{(\rho_0 + \alpha\rho_0 - \alpha - \alpha^2\cos\theta)^2 - (1-\alpha^2)[(\rho_0 + \alpha\rho_0 - \alpha)^2 - \alpha^2]\}^{1/2} \tag{2.16}$$

for $0 \le \alpha < 1$. For the special case $v_A = v_B$ we have $\alpha = 1$ and

$$\rho(\theta) = 2\rho_0(\rho_0 - 1)(2\rho_0 - 1 - \cos\theta)^{-1} , \tag{2.17}$$

which is a branch of a hyperbola.

The expression (2.15) is valid until the line $O'P$ becomes tangent to the A-B interface. For later times the line $O'P$ will not lie entirely in the A phase and a different approach must be used to find the curve $r = r(\theta)$. Referring to Fig. 3, we see that the condition for tangency is

$$\frac{1}{r}\frac{dr}{d\theta} = \frac{\mathcal{L}(PQ)}{\mathcal{L}(O'Q)} = \frac{r - R\cos\theta}{R\sin\theta}$$

or

$$\rho\frac{d\theta}{d\rho} = \frac{\sin\theta}{\rho - \cos\theta} , \tag{2.18}$$

where $\mathcal{L}(x)$ is the length of x. We now differentiate Eq. (2.14) with respect to ρ to obtain

$$\rho\sin\theta\frac{d\theta}{d\rho} = \alpha^{-1}[\alpha^{-1}(\rho - \rho_0) + 1 - \rho_0] - \rho + \cos\theta . \tag{2.19}$$

Combining Eqs. (2.18) and (2.19), we have

$$\alpha^{-1}(\rho - \cos\theta)[\alpha^{-1}(\rho - \rho_0) + 1 - \rho_0] = \rho^2 - 2\rho\cos\theta + 1 .$$

Finally, Eq. (2.14) can be inserted in this to yield

$$\alpha^{-1}(\rho - \cos\theta)[\alpha^{-1}(\rho - \rho_0) + 1 - \rho_0] = [\alpha^{-1}(\rho - \rho_0) + 1 - \rho_0]^2 . \tag{2.20}$$

At the point of tangency we must have $\theta > 0$, so $\rho(\theta) > \rho_0$ and

$$\alpha^{-1}(\rho - \rho_0) + 1 - \rho_0 > 0 .$$

Equation (2.20) now yields the angle θ_T at which the line $O'P$ is tangent to the A-B interface:

$$\theta_T = \cos^{-1}(\rho_0 + \alpha\rho_0 - \alpha) . \tag{2.21}$$

For the special case $\alpha = 1$ we have $\cos\theta_T = 2\rho_0 - 1$. Equation (2.17) then shows that $r(\theta_T) = \infty$, so Eq. (2.17) applies for all finite r and the entire interface is a branch of a hyperbola. For $\alpha < 1$, however, $r_T \equiv r(\theta_T)$ is finite, and we must obtain the form of the A-B interface for $\theta > \theta_T$. Once the tangent point T has been reached, the line OP is still contained in the B phase, but the shortest path from P to O' which lies entirely within the A phase runs along the interface from P to T, and then straight to O' (Fig. 4). Thus, for $\theta > \theta_T$ we have

$$v_B^{-1}[r(\theta) - r_T] = v_A^{-1}\mathcal{L}(\text{arc}PT) = v_A^{-1}\int_{\theta_T}^{\theta}\left[\left[\frac{dr}{d\theta'}\right]^2 + r^2\right]^{1/2} d\theta' .$$

Differentiation with respect to θ then yields

$$\frac{dr}{d\theta} = \alpha\left[\left[\frac{dr}{d\theta}\right]^2 + r^2\right]^{1/2} . \tag{2.22}$$

The required solution to Eq. (2.22) is a logarithmic spiral:

$$r(\theta) = r_T\exp\left[\frac{\alpha}{(1-\alpha^2)^{1/2}}(\theta - \theta_T)\right] \quad \text{for} \quad \theta \ge \theta_T . \tag{2.23}$$

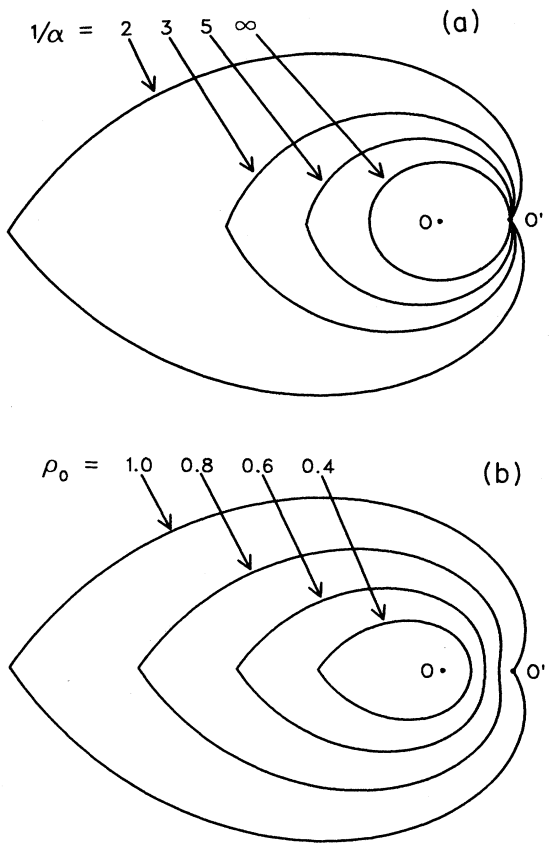

FIG. 5. (a) Shape of the A-B interface at $t=\infty$ for $\rho_0=1$ and $\alpha^{-1}=2$, 3, 5, and ∞. (b) Shape of the A-B interface at $t=\infty$ for $\alpha=0.5$ and $\rho_0=0.4$, 0.6, 0.8, and 1.0. In both (a) and (b), the nuclei of the A- and B-phase grains are at O' and O, respectively.

Note that at $\theta=\pi$ symmetric segments of logarithmic spirals meet to form a cusp. The shape of the A-B interface at $t=\infty$ is shown for several values of α and ρ_0 in Fig. 5.

In Fig. 4, the line segment ST has the same length as the arc PT which runs along the interface. This means that the growth of the A phase is retarded in the vicinity of the point P. It is not difficult to obtain a parametric equation describing the retarded portion of the interface between the metastable and A phases, i.e., the arc SP. This enables us to show a sequence of snapshots of the collision of the A and B grains (Fig. 6).

We can now understand the nature of the mean-field approximations. For simplicity, let us consider the case of heterogeneous nucleation for $\alpha<1$. The approximate result (2.4) for the untransformed fraction Φ can be interpreted as follows: According to Eq. (2.4), an arbitrary point P_1 is untransformed at time t if there are no A-phase nuclei within a distance $v_A t$ of P_1 and if there are no B-phase nuclei within a distance $v_B t$ of P_1. This is not exact because it does not take into account the retardation of the A-phase grains through collisions with B-phase grains. If $\alpha=1$, on the other hand, the condition for tangency is never attained and there is no retardation effect. The MFT is therefore exact for this case. A similar discussion applies for homogeneous nucleation.

The retardation of A-phase growth through collisions with B-phase grains has the effect of reducing the fraction in the A phase below the mean-field results (2.5) and (2.11). Equations (2.5) and (2.11) are therefore exact upper bounds on the A-phase fractions for heterogeneous and homogeneous nucleation, respectively.

As usual, MFT is expected to become an increasingly good approximation as the dimension of space d is increased. The retardation effect is very marked in $d=1$, since a B-phase grain completely arrests the growth of one of the two point interfaces of an A-phase grain. As we have seen, retardation is less pronounced in $d=2$, so we expect that the MFT will be a better approximation in 2D than in 1D. This expectation is borne out by the analytical and Monte Carlo work reported below.

III. EXACT SOLUTIONS IN ONE DIMENSION

It is useful to study two-phase nucleation and growth in 1D, since exact solutions are possible in this case. Behavior which is qualitatively different from the mean-field predictions emerges in one dimension.

A. Heterogeneous nucleation

Consider first the simpler case of heterogeneous nucleation. As a preliminary step, we study a different "one-sided" problem in which no nuclei are placed to the left of the origin. Nuclei are scattered to the right of the origin just as in the original problem. Let $p_A(t)$ be the probability that the origin is transformed before time t by

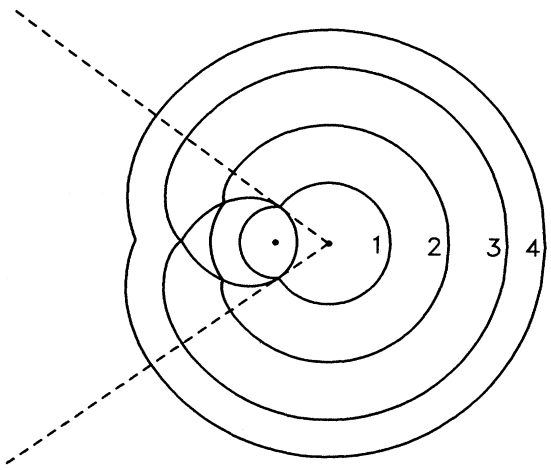

FIG. 6. A sequence of snapshots of the collision of the A- and B-phase grains. 1, 2, 3, and 4 show the grain interfaces at times $t_1,\ldots,t_4$, where $t_1<t_2<t_3<t_4$. The tangency condition Eq. (2.21) is satisfied at time $t=t_1$. The A-phase grain has just enveloped the B-phase grain at time $t=t_3$. The dashed rays radiate from the A-phase nucleus and are tangent to the A-B interface at $t=\infty$. Retardation of the growth of the A-phase grain occurs within the wedge enclosed by the dashed lines.

an A-phase grain. The probability $p_B(t)$ is similarly defined. The origin is transformed by an A-phase grain between times t and $t+dt$ only if an A-phase nucleus lies in the interval

$$x \in [v_A t,\ v_A(t+dt)]$$

and if no A- or B-phase nuclei lie in the interval $x \in (0, v_A t)$. Thus

$$\dot{p}_A(t)dt = \gamma_A v_A dt \exp[-(\gamma_A+\gamma_B)v_A t] . \quad (3.1)$$

Integrating this with respect to time and using the initial condition $p_A(0)=0$, we obtain

$$p_A(t) = \frac{\gamma_A}{\gamma_A+\gamma_B}\{1-\exp[-(\gamma_A+\gamma_B)v_A t]\} . \quad (3.2)$$

Similarly,

$$p_B(t) = \frac{\gamma_B}{\gamma_A+\gamma_B}\{1-\exp[-(\gamma_A+\gamma_B)v_B t]\} . \quad (3.3)$$

The probability that the origin is in the metastable phase at time t is

$$\phi(t) \equiv 1-p_A(t)-p_B(t)$$

$$= \frac{\gamma_A}{\gamma_A+\gamma_B}\exp[-(\gamma_A+\gamma_B)v_A t] + \frac{\gamma_B}{\gamma_A+\gamma_B}\exp[-(\gamma_A+\gamma_B)v_B t] . \quad (3.4)$$

We now return to the original "two-sided" problem. In the time interval $[t,t+dt]$ the origin may be transformed by the growth of an A-phase grain which nucleated to the right, provided that the origin has not previously been transformed by an A- or B- phase grain which nucleated to the left. The origin may also be transformed by an A-phase grain which nucleated to the left. The fraction of material in the A phase at time t is therefore given by

$$\dot{n}_A(t) = 2\phi(t)\dot{p}_A(t) . \quad (3.5)$$

Inserting Eqs. (3.1) and (3.4) into this and integrating, we obtain

$$n_A(t) = \frac{\gamma_A^2}{(\gamma_A+\gamma_B)^2}\{1-\exp[-2(\gamma_A+\gamma_B)v_A t]\} + 2\frac{\gamma_A\gamma_B}{(\gamma_A+\gamma_B)^2}\frac{v_A}{v_A+v_B}\{1-\exp[-(\gamma_A+\gamma_B)(v_A+v_B)t]\} . \quad (3.6)$$

In particular,

$$n_A(\infty) = \frac{\gamma_A^2}{(\gamma_A+\gamma_B)^2} + 2\frac{\gamma_A\gamma_B}{(\gamma_A+\gamma_B)^2}\frac{v_A}{v_A+v_B} . \quad (3.7)$$

This result is easily understood. The first term on the right-hand side of Eq. (3.7) is the probability that the nuclei which are closest to the origin on its right and left are both in the A phase. The second term gives the probability that one of the two closest nuclei is in the B phase, but that the A-phase grain reaches the origin first. Finally, an argument similar to that used to obtain Eq. (3.5) shows that the total fraction of untransformed material at time t is

$$\Phi(t) = \phi^2(t) . \quad (3.8)$$

Referring to Eq. (3.4), we see that since $v_B \le v_A$,

$$\Phi(t) \sim \exp[-2(\gamma_A+\gamma_B)v_B t] \quad \text{as} \quad t \to \infty . \quad (3.9)$$

This is the same as if we had replaced γ by $\gamma_A+\gamma_B$ and v by v_B in the $d=1$ version of the one-phase result Eq. (1.2). Also note that the true asymptotic decay of $\Phi(t)$ is slower than predicted by the MFT unless $v_A = v_B$ [see Eq. (2.4)].

The exact result for $n_A(\infty)$, Eq. (3.7), is compared with the mean-field prediction (2.6) in Fig. 7, for several values of

$$\eta_A \equiv \gamma_A/(\gamma_A+\gamma_B) .$$

As already remarked, the mean-field result is exact in the limit $\alpha \to 1$, and is greater than or equal to the exact value of $n_A(\infty)$ for all values of the parameters. The mean-field approximation is poor when α and η_A are small.

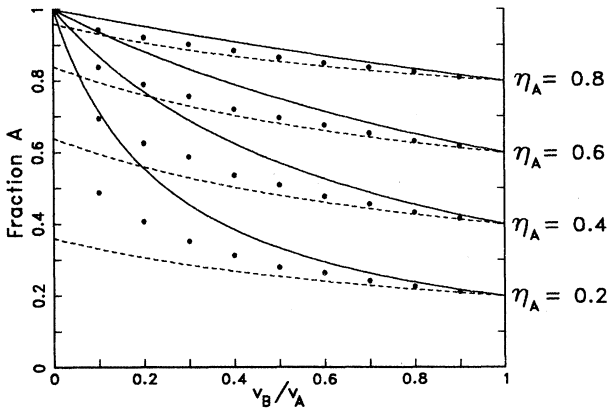

FIG. 7. The fraction of material in the A phase at time $t=\infty$ for heterogeneous and homogeneous nucleation in 1D. The parameter η_A is defined to be $\gamma_A/(\gamma_A+\gamma_B)$ for heterogeneous nucleation and $\Gamma_A/(\Gamma_A+\Gamma_B)$ for homogeneous nucleation. The mean-field results for heterogeneous and homogeneous nucleation are identical when expressed in terms of η_A and are shown with solid lines for $\eta_A=0.2$, 0.4, 0.6, and 0.8. For each of these values of η_A, the exact results for heterogeneous nucleation (dashed lines) and the Monte Carlo results for homogeneous nucleation (solid circles) are shown.

B. Homogeneous nucleation

We now turn to homogeneous two-phase nucleation and growth in 1D. It is again convenient to first study a "one-sided" problem in which nucleation occurs as usual to the right of the origin but does not occur to the left. We define p_A, p_B, and ϕ as in Sec. III A. Thus, $\dot{p}_A(t)dt$ is the probability that the origin is transformed between time t and $t+dt$ by an A-phase grain. Such a grain can have nucleated at any point x in the interval $0 \le x \le v_A t$ between times $t - x/v_A$ and $t - x/v_A + dt$. Hence

$$\dot{p}_A(t)dt = \int_0^{v_A t} \Gamma_A dx\, dt \phi\left[t - \frac{x}{v_A}\right] \times \exp\left[-(\Gamma_A+\Gamma_B)\left[t - \frac{x}{2v_A}\right]x\right] . \tag{3.10}$$

Here,

$$\Gamma_A dx\, dt \phi(t - x/v_A)$$

is the probability that an A-phase nucleus appears in the interval $[x, x+dx]$ between times $t - x/v_A$ and $t - x/v_A + dt$. This can occur only if the interval $[x, x+dx]$ was not previously transformed—hence the factor $\phi(t - x/v_A)$. The exponential factor in Eq. (3.10) ensures that a second grain does not prevent the A-phase grain with a nucleus in $[x, x+dx]$ from reaching the origin. Changing variables from x to $s \equiv t - x/v_A$ in Eq. (3.10), we obtain

$$\dot{p}_A(t) = \Gamma_A v_A \int_0^t \exp[-\tfrac{1}{2}(\Gamma_A+\Gamma_B)v_A(t^2-s^2)]\phi(s)ds . \tag{3.11}$$

In the same way,

$$\dot{p}_B(t) = \Gamma_B v_B \int_0^t \exp[-\tfrac{1}{2}(\Gamma_A+\Gamma_B)v_B(t^2-s^2)]\phi(s)ds . \tag{3.12}$$

Addition of Eqs. (3.11) and (3.12) yields

$$\dot{\phi}(t) = -\int_0^t \{\Gamma_A v_A \exp[-\tfrac{1}{2}(\Gamma_A+\Gamma_B)v_A(t^2-s^2)] + \Gamma_B v_B \exp[-\tfrac{1}{2}(\Gamma_A+\Gamma_B)v_B(t^2-s^2)]\}\phi(s)ds , \tag{3.13}$$

which is a closed integrodifferential equation for ϕ.

To solve Eq. (3.13), we first convert it to a differential equation. This is accomplished by multiplying both sides of (3.13) by $\exp[\frac{1}{2}(\Gamma_A+\Gamma_B)v_A t^2]$ and differentiating with respect to t. The resultant equation may be written as

$$t^{-1}\exp[\tfrac{1}{2}(\Gamma_A+\Gamma_B)v_B t^2][\ddot{\phi}(t) + (\Gamma_A+\Gamma_B)v_A t\dot{\phi}(t) + (\Gamma_A v_A + \Gamma_B v_B)\phi(t)] = -\Gamma_B v_B(\Gamma_A+\Gamma_B)(v_A - v_B)\int_0^t \exp[\tfrac{1}{2}(\Gamma_A+\Gamma_B)v_B s^2]\phi(s)ds . \tag{3.14}$$

Differentiating once more, we obtain the third-order ordinary differential equation

$$t\frac{d^3\phi}{dt^3} + [(\Gamma_A+\Gamma_B)(v_A+v_B)t^2 - 1]\frac{d^2\phi}{dt^2} + [(\Gamma_A+\Gamma_B)^2 v_A v_B t^3 + (\Gamma_A v_A + \Gamma_B v_B)t]\frac{d\phi}{dt} + [(\Gamma_A+\Gamma_B)^2 v_A v_B t^2 - (\Gamma_A v_A + \Gamma_B v_B)]\phi = 0 . \tag{3.15}$$

Our new step will be to construct a first integral of Eq. (3.15). Note that if we set

$$F(t) \equiv \ddot{\phi} + (\Gamma_A+\Gamma_B)(v_A+v_B)t\dot{\phi} + [(\Gamma_A+\Gamma_B)^2 v_A v_B t^2 + (\Gamma_A v_A + \Gamma_B v_B)]\phi ,$$

then (3.15) may be written

$$t\dot{F} = F . \tag{3.16}$$

This is readily integrated to give $F(t) = kt$, where k is a constant. Since $\phi(t)$ approaches zero rapidly as $t \to \infty$, we must have $k = 0$. We then have the desired first integral $F = 0$ or

$$\ddot{\phi} + (\Gamma_A+\Gamma_B)(v_A+v_B)t\dot{\phi} + [(\Gamma_A+\Gamma_B)^2 v_A v_B t^2 + (\Gamma_A v_A + \Gamma_B v_B)]\phi = 0 . \tag{3.17}$$

Equation (3.17) may be reduced to standard form by setting

$$\phi = \exp[-\tfrac{1}{4}(\Gamma_A+\Gamma_B)(v_A+v_B)t^2]\psi .$$

We obtain

$$\frac{d^2\psi}{d\tau^2} = (\tfrac{1}{4}\tau^2 + a)\psi , \tag{3.18}$$

where

$$\tau \equiv [(\Gamma_A+\Gamma_B)(v_A - v_B)]^{1/2} t$$

and

$$a \equiv -\frac{1}{2}\frac{\Gamma_A - \Gamma_B}{\Gamma_A + \Gamma_B} .$$

The solution to Eq. (3.18) which satisfies the initial condition $\psi(0)=1$ is the even parabolic cylinder function[16]

$$\psi(\tau) = e^{-\tau^2/4} M(\tfrac{1}{2}a + \tfrac{1}{4}, \tfrac{1}{2}, \tfrac{1}{2}\tau^2) ,$$

wher M is Kummer's function.[17] We conclude that

$$\phi(t) = \exp[-\tfrac{1}{2}(\Gamma_A + \Gamma_B) v_A t^2] \times M(\tfrac{1}{2}a + \tfrac{1}{4}, \tfrac{1}{2}, \tfrac{1}{2}(\Gamma_A + \Gamma_B)(v_A - v_B)t^2) . \quad (3.19)$$

The fraction in the metastable phase at time t in the original "two-sided" problem is $\Phi(t) = \phi^2(t)$. Explicitly,

$$\Phi(t) = \exp[-(\Gamma_A + \Gamma_B) v_A t^2] \times M^2(\tfrac{1}{2}a + \tfrac{1}{4}, \tfrac{1}{2}, \tfrac{1}{2}(\Gamma_A + \Gamma_B)(v_A - v_B)t^2) . \quad (3.20)$$

For $v_A = v_B \equiv v$, this reduces to the one-phase result Eq. (1.1) with $\Gamma = \Gamma_A + \Gamma_B$, as it must. For $v_B < v_A$, the asymptotic behavior of $\Phi(t)$ as $t \to \infty$ is

$$\Phi(t) \sim \exp[-(\Gamma_A + \Gamma_B) v_B t^2] t^{-\nu} , \quad (3.21)$$

where

$$\nu \equiv \frac{2}{1+\bar{\Gamma}} .$$

Here we have used the fact that $M(x,y,z) \sim e^z z^{x-y}$ as $z \to \infty$ with x and y fixed.[17]

The decay of $\Phi(t)$ for large t is slower than predicted by mean-field theory if $v_B < v_A$. Also, the leading-order asymptotic behavior of Φ in the two-phase model is the same as the one-phase result Eq. (1.1) for $d=1$ with Γ replaced by $\Gamma_A + \Gamma_B$ and v replaced by the smaller of v_A and v_B, namely, v_B. These observations are completely analogous to those made previously for heterogeneous nucleation in 1D. The power-law correction $t^{-\nu}$ to the exponential decay of $\Phi(t)$ is a new feature which does not appear in the MFT. Interestingly, the exponent ν varies continuously as a function of $\bar{\Gamma} \equiv \Gamma_B / \Gamma_A$.

In the limit $v_B \to 0$, we have the surprising result

$$\Phi(t) \sim t^{-\nu} \text{ as } t \to \infty .$$

Thus, when $v_B = 0$ material is transformed much more slowly in the two-phase model than in the one-phase model. This is to be expected since if $v_B = 0$, the increasing number of B-phase nuclei serve only to impede the transformation of material by the growth of A grains. Of course, for any $v_B > 0$ crossover from power-law decay to the rapid decay

$$\Phi(t) \sim \exp[-(\Gamma_A + \Gamma_B) v_B t^2]$$

will occur at times on the order of

$$(\Gamma_A + \Gamma_B)^{-1/2} v_B^{-1/2} .$$

Anomalous kinetics of this kind are not expected in homogeneous two-phase nucleation and growth with $v_B = 0$ in higher dimensions d, since point nuclei of B phase stop the growth of A-phase grains only in 1D.

The fraction of material in the A phase at time t is

$$n_A(t) = 2\Gamma_A v_A \int_0^t ds_1 \int_0^{s_1} ds_2 \exp[-\tfrac{1}{2}(\Gamma_A + \Gamma_B) v_A (s_1^2 - s_2^2)] \phi(s_1)\phi(s_2) ,$$

where Eqs. (3.5) and (3.11) have been employed. Equation (3.19) for ϕ can now be plugged into this to yield a closed expression for $n_A(t)$. Unfortunately, we have not been able to evaluate the resultant double integral analytically, even in the limit $t = \infty$. Rather than numerically evaluate the double integral for different parameter values, we found it simplest to find $n_A(\infty)$ by a Monte Carlo simulation.

Performing a Monte Carlo simulation of 1D homogeneous nucleation is straightforward. Our algorithm proceeds as follows: First we generate the time until the next possible nucleation event. This quantity follows a simple exponentially decreasing probability distribution which depends on the sum of the two nucleation rates. The space coordinate for the event is selected from a uniform distribution over the finite size of the system. This coordinate is then checked to see whether it falls in an untransformed region at the time of the nucleation event. If so, a new grain is formed. The phase of the grain is chosen randomly, based on the relative nucleation rates of the two species. If the site has already been transformed, on the other hand, the event is simply discarded. This process continues until the entire finite interval has been transformed, after which the fractions in the two phases are calculated. Finally, the simulation is repeated to gather statistical information.

A number of structures were used to increase the efficiency of the calculation. In particular, the basic data structure for describing the system at any time is a set of the open intervals available for nucleation. These intervals contain information on the velocities of the fronts as well as information as to when the interval will close up. This set is organized as a binary tree to provide a fast means of checking whether a given point falls into one of the intervals. The information on front collision times is also stored in a binary tree to provide an efficient means for eliminating null intervals.

The size of the system was varied to provide about 10 000 actual nucleation events in each simulation. This was found to make the finite size effect negligible relative to the statistical errors. Ten simulations were performed for each data point, to provide an estimate of the statisti-

cal fluctuations. The results are presented in Fig. 7 for several values of

$$\eta_A = \Gamma_A/(\Gamma_A+\Gamma_B) ,$$

along with the mean-field prediction. As expected, the Monte Carlo results fall below the values predicted by the mean-field theory.

IV. MONTE CARLO RESULTS IN TWO DIMENSIONS

From our geometric results on the collision of a single pair of grains in two dimensions, it is clear that a simulation of a system of growing and colliding disks would be difficult. In lieu of this, we have performed Monte Carlo simulations of nucleation and growth in 2D for diamond-shaped grains. To be precise, we employed the Manhattan metric in which the distance between two points (x_1,y_1) and (x_2,y_2) is

$$d_{12} = |x_1-x_2|+|y_1-y_2| ,$$

whereas in our earlier work the Euclidean metric

$$d_{12} = [(x_1-x_2)^2+(y_1-y_2)^2]^{1/2}$$

was used. At time t, therefore, the boundary of a single A-phase grain which nucleated at the origin at time $t=0$ is given by $|x|+|y|=v_A t$. A similar expression holds for a B-phase grain. As they were previously, A-B interfaces are treated as stationary. Note that the grain boundaries in these models are straight lines, even after two or more grains have collided. This simplifies the Monte Carlo simulation enormously.

The mean-field theories for heterogeneous and homogeneous nucleation are easily modified to apply to the problems with growing diamonds. The results are given by Eqs. (2.6) and (2.12) with $d=2$, and are the same as for growing disks. Note that the retardation effect is still present in our modified problems, so the mean-field theories are only exact for $v_A=v_B$.

A. Heterogeneous nucleation

To simulate heterogeneous nucleation in two dimensions, we distributed 100 nucleation sites in a square of side 1000 with periodic boundary conditions. Although these sites were constrained to lie on a square grid with unit lattice spacing, the subsequent evolution was calculated in the continuum. The details of the algorithm are presented in the following paragraphs. The simulation was repeated ten times for each set of nucleation rates and velocities. An example of a completely transformed system is shown in Fig. 8. The Monte Carlo results for $n_A(\infty)$ are shown in Fig. 9 for several different values of

$$\eta_A \equiv \gamma_A/(\gamma_A+\gamma_B) ,$$

and are compared to the mean-field prediction Eq. (2.6). The data are very close to the mean-field results, but are consistently below the latter by about one standard deviation. As expected, the MFT is a much better approximation in two dimensions than in one.

The key element in the simulation is the observation that the moving grain boundaries are line segments parallel to either $x=y$ or $x=-y$. The stationary A-B grain boundaries are also linear, but with slopes depending on the relative velocities of the species. The primary data structures we employed were two sorted lists of the moving boundaries, one for boundaries with constant $x+y$ ordered according to the value of $x+y$, and the other for boundaries with constant $x-y$ ordered according to the value of $x-y$.

There are two types of events which can alter the structure of these lists. One event corresponds to the passing (or collision) of two parallel boundary segments moving in opposite directions. The other event corresponds to the disappearance of a boundary segment which has been shrinking in size. The time to the earliest event of either type is calculated in a single pass through

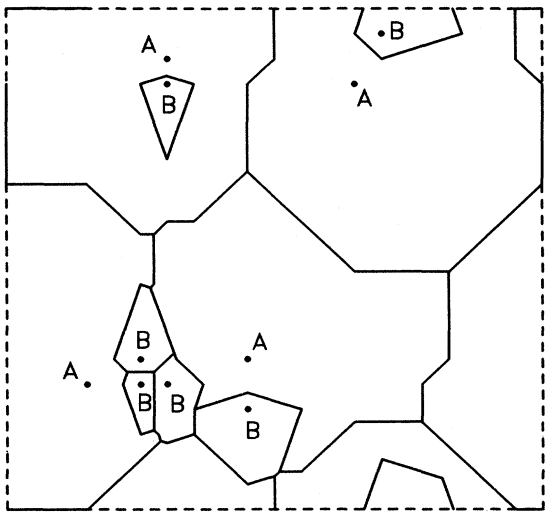

FIG. 8. An example of the grain geometry at $t=\infty$ for heterogeneous nucleation with $v_B/v_A=0.5$. In this case there are four A-phase grains and six B-phase grains.

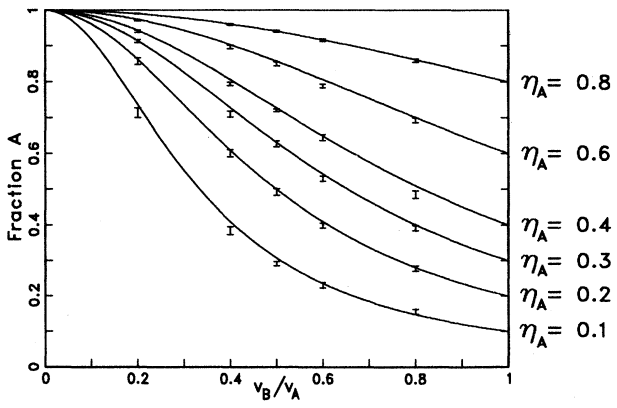

FIG. 9. The fraction of material in the A phase at time $t=\infty$ for heterogeneous nucleation in 2D. The mean-field curves (solid lines) and Monte Carlo results (vertical bars) are shown for $\eta_A=0.1$, 0.2, 0.3, 0.4, 0.6, and 0.8.

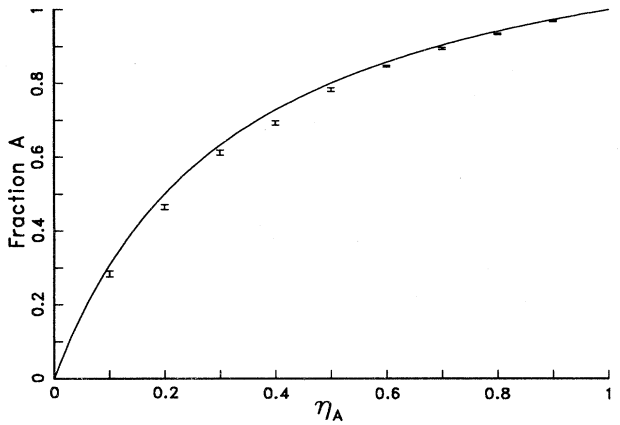

FIG. 10. The fraction of material in the A phase at time $t=\infty$ for homogeneous nucleation in 2D with $\alpha=\frac{1}{2}$. The solid curve is the mean-field prediction, while the vertical bars give the Monte Carlo results.

the lists. The segments are then updated to the new time, and the area of each grain is incremented (by the amount enclosed by the trapezoid formed between the old and new location of a grain boundary segment). Finally, the lists are updated to reflect the effects of the various changes in ordering, collisions, and disappearances. The process continues until the lists of moving boundaries are empty and the entire area of the system has been transformed.

To avoid precision problems, all quantities in the simulation were represented as rational numbers. This was possible because the positions of the nuclei were on a lattice and the velocities were chosen to have a ratio of small integers. The algorithmic does not depend on either condition, but the roundoff errors necessitate these choices.

B. Homogeneous nucleation

As a result of the precision problems involved with real number calculations, it was not possible to extend the approach we used for heterogeneous nucleation to the homogeneous case. To obtain Monte Carlo data for this case, we discretized both space and time and fixed the velocity ratio α at $\frac{1}{2}$. The simulation involved two stages at each time step. In the first stage, a nucleus could form at each untransformed site with a probability proportional to the total nucleation rate. In the second stage, one of the species was selected to grow. To obtain a velocity ratio of $\frac{1}{2}$, the B phase was chosen once every three steps. Each untransformed site adjacent to the growing phase was then occupied by that phase.

Simulations were performed on an 800×800 square lattice with periodic boundary conditions. As mentioned previously, α was fixed at $\frac{1}{2}$. The total nucleation rate per time step was adjusted so that approximately 1000 nucleation events occurred for each simulation. Ten simulations were performed for each data point. The results are shown in Fig. 10, along with the mean-field prediction [Eq. (2.12)]. The results are once again close to the mean-field prediction (and below it), but they appear somewhat farther away than the heterogeneous case. Part of this difference is due to a small systematic bias in favor of the slower B phase in the discretized version of the problem. A more careful justification of our Monte Carlo approach can be given by arguing that our results provide a lower bound on the actual value of $n_A(\infty)$, however. In any case, the Monte Carlo simulation again supports our view that the MFT becomes an increasingly good approximation as d is increased.

V. CONCLUSIONS

In this paper we have studied nucleation and growth in systems with two distinct stable phases, A and B. Both homogeneous and heterogeneous nucleation were considered. Our first step was to develop mean-field theories for these problems which give the fraction of material in the A phase at time t, $n_A(t)$. We then showed that during the collision of an A- and a B-phase grain, the growth of the faster-growing A-phase grain is retarded. This led us to conclude that the mean-field theories are exact only in the $v_A=v_B$ limit. For $v_A>v_B$, the mean-field result for $n_A(t)$ is an upper bound on the exact result, however. We then solved the homogeneous and heterogeneous nucleation and growth problems exactly in one dimension. The mean-field theories give poor approximations for $n_A(\infty)$ in 1D, except in the limit $v_A/v_B\to1$. In addition, we find an anomalous power-law correction to the leading-order exponential decay of the untransformed fraction $\Phi(t)$ in homogeneous 1D nucleation and growth. The power-law exponent is a continuously varying function of the nucleation rates. Nothing of this kind appears in the mean-field theory.

As usual, we expect the mean-field theories to become increasingly good approximations as the spatial dimension d is increased. This expectation is supported by our Monte Carlo simulations of heterogeneous and homogeneous nucleation in two dimensions. Indeed, we found that the mean-field results provide a surprisingly accurate approximation for $n_A(\infty)$ in $d=2$.

In closing, we would like to remark that many of the results reported here are easily generalized to systems with three or more distinct stable phases.

ACKNOWLEDGMENTS

We would like to thank J.-M. Debierre, R. C. Desai, R. D. Etters, J. M. E. Harper, K. F. Ludwig, and D. A. Smith for useful discussions. R.M.B. is grateful to IBM for financial support of this work.

[1]A. N. Kolmogorov, Izv. Akad. Nauk SSSR, Ser. Fiz. **3**, 355 (1937).
[2]W. A. Johnson and R. F. Mehl, Trans. Am. Inst. Min. Metall. Pet. Eng. **135**, 416 (1939).
[3]M. Avrami, J. Chem. Phys. **7**, 1103 (1939); **8**, 212 (1939); **9**, 177 (1941).
[4]J. W. Christian, *The Theory of Transformations in Metals and Alloys* (Pergamon, Oxford, 1965).
[5]K. N. Tu, D. A. Smith, and B. Z. Weiss, Phys. Rev. B **36**, 8948 (1987).
[6]B. C. Sales, J. O. Ramsey, and L. A. Boatner, Phys. Rev. Lett. **59**, 1718 (1987).
[7]A. P. Radlinski, A. Calka, and B. Luther-Davies, Phys. Rev. Lett. **57**, 3081 (1986).
[8]J. D. Axe and Y. Yamada, Phys. Rev. B **34**, 1599 (1986).
[9]K. Sekimoto, Physica **A135**, 328 (1986).
[10]S. Ohta, T. Ohta, and K. Kawasaki, Physica **A140**, 478 (1987).
[11]Y. Yamada, N. Hamaya, J. D. Axe, and S. M. Shapiro, Phys. Rev. Lett. **53**, 1665 (1984).
[12]N. Hamaya, Y. Yamada, J. D. Axe, D. P. Belanger, and S. M. Shapiro, Phys. Rev. B **33**, 7770 (1986).
[13]Y. Ishibashi and Y. Takagi, J. Phys. Soc. Jpn. **31**, 506 (1971).
[14]K. Dimmler, M. Parris, D. Butler, S. Eaton, B. Pouligny, J. F. Scott, and Y. Ishibashi, J. Appl. Phys. **61**, 5467 (1987).
[15]The special case of homogeneous nucleation with $\Gamma_A = \Gamma_B$ and $v_A = v_B$ has been studied previously by Ohta *et al.* (Ref. 10).
[16]J. C. P. Miller, in *Handbook of Mathematical Functions,* edited by M. Abramowitz and I. A. Stegun (U.S. GPO, Washington, D.C., 1972), Chap. 19.
[17]L. J. Slater, in *Handbook of Mathematical Functions,* Ref. 16, Chap. 13.